

# Engineered three-dimensional cardiac tissues maturing in a rotating wall vessel bioreactor remodel diseased hearts in rats with myocardial infarction

Taro Nakazato,<sup>1</sup> Takuji Kawamura,<sup>1</sup> Toshimasa Uemura,<sup>2,3</sup> Li Liu,<sup>1</sup> Junjun Li,<sup>1</sup> Masao Sasai,<sup>1</sup> Akima Harada,<sup>1</sup> Emiko Ito,<sup>1</sup> Hiroko Iseoka,<sup>1</sup> Koichi Toda,<sup>1</sup> Yoshiki Sawa,<sup>1</sup> and Shigeru Miyagawa<sup>1,\*</sup>

<sup>1</sup>Department of Cardiovascular Surgery, Osaka University Graduate School of Medicine, Suita, Osaka, Japan

<sup>2</sup>Department of Precise and Science Technology, Osaka University Graduate School of Engineering, Suita, Osaka, Japan

<sup>3</sup>Cell Culture Marketing & Research Center, JTEC Corporation, Ibaraki, Osaka, Japan

\*Correspondence: [miya-p@surg1.med.osaka-u.ac.jp](mailto:miya-p@surg1.med.osaka-u.ac.jp)

<https://doi.org/10.1016/j.stemcr.2022.03.012>

## SUMMARY

A rotating wall vessel (RWV) bioreactor was constructed for growing massive functional cardiac constructs to recover the function of a distressed rat heart. Three-dimensional cardiac tissues were engineered by seeding human-induced pluripotent stem cell-derived cardiomyocytes on poly(lactic-co-glycolic acid) fiber sheets (3D-hiPSC-CTs) and cultured in the RWV bioreactor (RWV group) or under static conditions (control group). The tissues were transplanted into a myocardial infarction nude rat model, and cardiac performance was evaluated. In the RWV group, cell viability and contractile and electrical properties significantly improved, mature cardiomyocytes were observed, and mechanical stress-related mediators of mammalian target of rapamycin signaling were upregulated compared with those of the control. Four weeks post-transplantation, tissue survival and left ventricular ejection fraction significantly improved in the RWV group. Hence, dynamic culture in an RWV bioreactor could provide a superior culture environment for improved performance of 3D-hiPSC-CTs, providing a means for functional cardiomyogenesis in myocyte-loss heart failure.

## INTRODUCTION

Severe heart failure, leaving only a few functional cardiomyocytes (CMs), is clinically challenging (Lee et al., 2009); regenerative therapy offers a new strategy for treating severely damaged myocardia. However, the human left ventricle (LV) contains approximately six billion CMs, one billion of which are expected to be required for achieving therapeutic effects beyond those obtained with conventional cytokine therapy (Tohyama et al., 2013). To successfully treat severe heart failure in which few functional CMs remain, construction and transplantation of an engineered mature three-dimensional (3D) cardiac tissue resembling the human myocardium with many functional CMs is crucial. Indeed, engineered tissue composed of stacking cell sheets or gelatin hydrogels may be a suitable source for such a large number of CMs. When constructing a 3D cardiac tissue *ex vivo*, generation of large cardiac tissues with preserved, or improved, function via regular supply of nutrients and oxygen to the whole tissue is an essential consideration. Generally, most culture methods for an engineered 3D cardiac tissue are static, which may lead to an insufficient supply of nutrients and oxygen delivered to the center of the tissue owing to its thickness (Shimizu et al., 2006). Hence, bioreactors capable of effectively delivering oxygen and nutrients to the center of thick cardiac tissue may be required to address this issue. Application of mechanical stimulation, such as stretching or shear stress

and electrical stimulation during culture have been reported to improve tissue functionality (Dvir et al., 2007; Godier-Furnémont et al., 2015; Imboden et al., 2019).

In this study, we employed a rotating wall vessel (RWV) bioreactor capable of maintaining a steady glucose concentration around the cultured tissue by ensuring regular culture media flow, while supplying both nutrients and oxygen effectively (Schwarz et al., 1992; Teo et al., 2014). This system also applies low shear stress to the cultured cells or tissue, leading to structural changes in the embryonic bodies and significant alteration of the gene expression profile (Sargent et al., 2010). In 2009, Sakai et al. (2009) successfully constructed a functional hyaline cartilage that was sufficiently large for clinical use. We hypothesized that dynamic culture in an RWV bioreactor would result in enhanced performance of engineered 3D cardiac tissue by effectively supplying the essential components for culture along appropriate shear stress, with minimal associated cellular damage, leading to superior therapeutic effects in a rat model of myocardial infarction (MI). To test this hypothesis, 3D cardiac tissues (CTs) were engineered by seeding human-induced pluripotent stem cell (hiPSC)-derived cardiomyocytes on poly(lactic-co-glycolic acid) fiber sheets and cultured in the RWV bioreactor (RWV group) or under static conditions (control group). The therapeutic effects of these 3D-hiPSC-CTs were then evaluated.

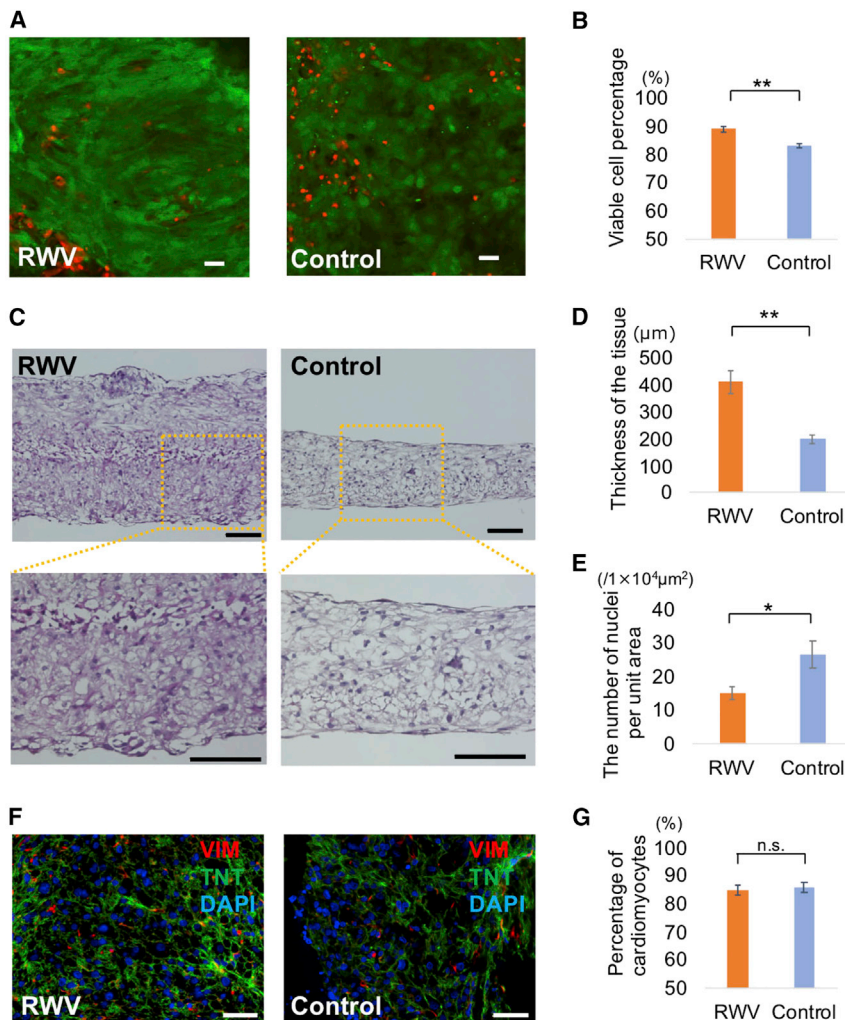


**Figure 1. Dynamic culture in a rotating wall vessel (RWV) bioreactor increases cell viability and thickness of a three-dimensional cardiac tissue derived from human-induced pluripotent stem cells (3D-hiPSC-CT)**

(A) Representative 3D-hiPSC-CT images in the cell viability assay. Nuclei of dead cells are stained red, and those of live cells are stained green. Scale bar, 50  $\mu\text{m}$ .

(B) Viable cell percentage (mean  $\pm$  SE) in 3D-hiPSC-CTs in the RWV and control groups (n = 3 per group). Independent experiments, one-tailed Student's *t* test. \*\*p < 0.01.

(C) Representative cross-section images of 3D-hiPSC-CTs stained with hematoxylin and eosin. Scale bar, 100  $\mu\text{m}$ .

(D) 3D-hiPSC-CT thickness (mean  $\pm$  SE) in the cross-section of the RWV and control groups (n = 4 per group). Independent experiments, one-tailed Student's *t* test. \*\*p < 0.01.

(E) Number of nuclei per unit area (mean  $\pm$  SE) in the hematoxylin and eosin-stained images of 3D-hiPSC-CTs in the RWV and control groups (n = 4 per group). Independent experiments, one-tailed Student's *t* test. \*p < 0.05.

(F) Representative immunostained images of 3D-hiPSC-CT; green = cardiac troponin T (TNT), red = vimentin (VIM), blue = DAPI. Scale bar, 50  $\mu\text{m}$ .

(G) Percentage of cardiomyocytes (mean  $\pm$  SE) in 3D-hiPSC-CT in the RWV and control groups (n = 5 per group). Independent experiments, one-tailed Student's *t* test. n.s., not significant.

## RESULTS

### Higher cell viability and thicker 3D-hiPSC-CTs in the RWV group

Cell viability was significantly higher in the RWV group (89%  $\pm$  0.9%) than in the control group (83%  $\pm$  0.9%; p = 0.0073; n = 3 per group; **Figures 1A and 1B**). Hematoxylin and eosin (H&E) staining of 3D-hiPSC-CTs cross-sections showed that the RWV group tissue was approximately twice as thick as that of the control group (413  $\pm$  42  $\mu\text{m}$  versus 201  $\pm$  16  $\mu\text{m}$ ; p = 0.0034; n = 4 per group; **Figures 1C and 1D**). Moreover, the RWV group had significantly fewer nuclei than the control group (26.5  $\pm$  4.1 versus 15.1  $\pm$  2.0/1.0  $\times 10^4 \mu\text{m}^2$ ; p = 0.0445; n = 4 per group; **Figure 1E**). Moreover, to evaluate the fraction of cardiomyocytes versus non-myocytes in 3D-hiPSC-CTs, we performed immunohistochemistry with cardiac troponin T (TNT) and vimentin. There was no significant difference

in the fraction of cardiomyocytes versus non-myocytes between the RWV group (85%  $\pm$  1.8%) and the control group (86%  $\pm$  1.8%; p = 0.8571; n = 5 per group; **Figure 1F**). For reference, the cell composition of non-myocytes before the generation of 3D-hiPSC-CTs is presented in the **supplemental information** (**Figure S1**). In addition, we performed immunohistochemistry for CD31 or smooth muscle actin (SMA) or TE-7, and we evaluated the cardiomyocyte fraction versus non-myocyte fraction (**Figure S2**). These findings collectively indicated that each cell on a 3D-hiPSC-CT sheet cultured in an RWV bioreactor may have grown larger than the cells cultured in static conditions.

### Dynamic culture in an RWV bioreactor promotes molecular and structural development of 3D-hiPSC-CTs

To evaluate cardiac-specific components in 3D-hiPSC-CTs, immunohistochemistry was performed. TNT-stained 3D-hiPSC-CTs are depicted in **Figure 2A**. In the RWV group,

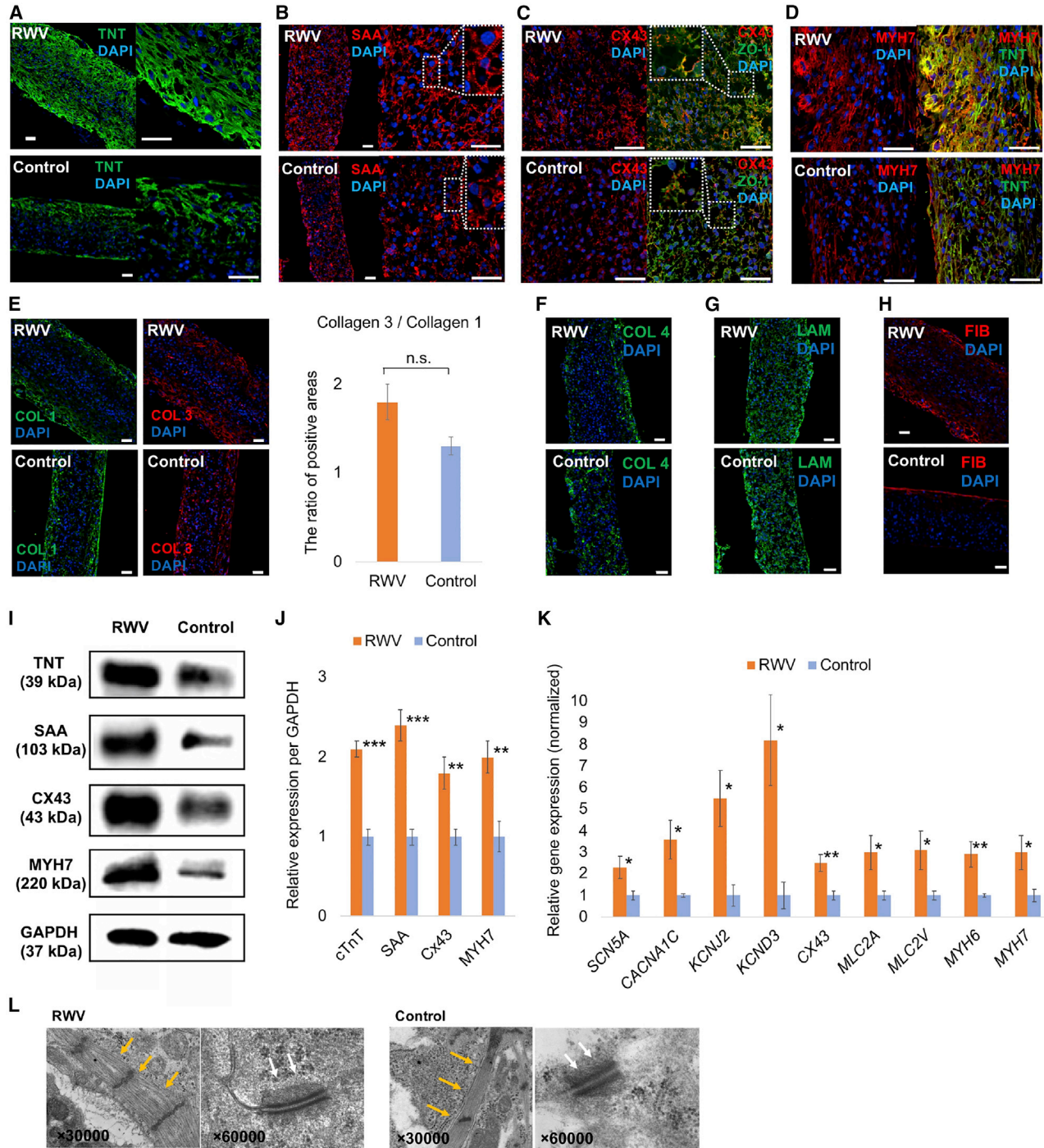


**Figure 2. Dynamic culture in a rotating wall vessel (RWV) bioreactor promotes molecular and structural development of a three-dimensional cardiac tissue derived from human-induced pluripotent stem cells (3D-hiPSC-CT)**

(A–D) Representative immunostained images of 3D-hiPSC-CTs: (A) green = cardiac troponin T (TNT); (B) red = sarcomeric  $\alpha$  actinin (SAA); (C) red = connexin 43 (CX43), green = zonula occludens-1 (ZO-1); (D) red = myosin heavy chain 7 (MYH7), green = cardiac troponin T (TNT), blue = DAPI. Scale bar, 50  $\mu$ m.

(E) Representative immunostained images of 3D-hiPSC-CTs: green = collagen 1 (Col 1), red = collagen 3 (Col 3), blue = DAPI. Scale bar, 50  $\mu$ m. The right graph shows the ratio of collagen 3 to collagen 1 positive areas (mean  $\pm$  SE) in the RWV and control groups (n = 6 per group). Independent experiments, one-tailed Student's *t* test. n.s., not significant.

(legend continued on next page)



the sarcomere structure was more clearly recognized when stained with sarcomeric  $\alpha$  actinin (SAA; Figure 2B). Double-staining with zonula occludens-1, a tight junction-associated protein, confirmed that connexin 43 (CX43) was expressed at the junction between cardiomyocytes in the RWV group (Figure 2C). Moreover, 3D-hiPSC-CTs were double-stained with TNT and myosin heavy chain 7 (MYH7; Figure 2D). Western blotting confirmed higher expression levels of TNT ( $2.1 \pm 0.1$  versus  $1.0 \pm 0.1$ ;  $p < 0.0001$ ;  $n = 5$  per group), SAA ( $2.4 \pm 0.2$  versus  $1.0 \pm 0.1$ ;  $p = 0.0003$ ;  $n = 5$  per group), CX43 ( $1.8 \pm 0.2$  versus  $1.0 \pm 0.1$ ;  $p = 0.0064$ ;  $n = 5$  per group), and MYH7 ( $2.0 \pm 0.2$  versus  $1.0 \pm 0.2$ ;  $p = 0.0071$ ;  $n = 5$  per group) in the RWV group than in the control group (expression levels were normalized to that of GAPDH; Figures 2I–2J). Additionally, we evaluated the extracellular matrix of 3D-hiPSC-CTs. In particular, we focused on the ratio of collagen 3 to collagen 1, which has been used as an indicator of pathological fibrosis of the myocardium (Polyakova et al., 2011). The ratio of the positive areas of collagen 3 to those of collagen 1 tended to be higher in the RWV group ( $1.8 \pm 0.2$  versus  $1.3 \pm 0.1$ ;  $p = 0.0808$ ;  $n = 6$  per group; Figure 2E). However, collagen 4 and laminin were similarly expressed in both groups (Figures 2F–2G). Fibronectin was expressed on both the upper and lower sides of a 3D-hiPSC-CT in the RWV group but was only expressed on one side in the control group (Figure 2H).

Regarding CM-specific mRNA expression, genes associated with ion channels, namely *SCN5A* ( $2.3 \pm 0.5$  versus  $1.0 \pm 0.2$ ;  $p = 0.043$ ;  $n = 5$  per group), *CACNA1C* ( $3.6 \pm 0.9$  versus  $1.0 \pm 0.1$ ;  $p = 0.023$ ;  $n = 5$  per group), *KCNJ2* ( $5.5 \pm 1.3$  versus  $1.0 \pm 0.5$ ;  $p = 0.0128$ ;  $n = 5$  per group), and *KCND3* ( $8.2 \pm 2.1$  versus  $1.0 \pm 0.6$ ;  $p = 0.0108$ ;  $n = 5$  per group), had significantly higher expression in the RWV group than in the control group. In addition, *CX43* ( $2.5 \pm 0.4$  versus  $1.0 \pm 0.2$ ;  $p = 0.0056$ ;  $n = 5$  per group), *myosin light chain (MLC) 2A* ( $3.0 \pm 0.8$  versus  $1.0 \pm 0.2$ ;  $p = 0.0477$ ;  $n = 5$  per group), *MLC2V* ( $3.1 \pm 0.9$  versus  $1.0 \pm 0.2$ ;  $p = 0.0453$ ;  $n = 5$  per group), *MYH6* ( $2.9 \pm 0.6$  versus  $1.0 \pm 0.1$ ;  $p = 0.0099$ ;  $n = 5$  per group), and *MYH7* ( $3.0 \pm 0.8$  versus  $1.0 \pm 0.3$ ;  $p = 0.049$ ;  $n = 5$  per group) showed signif-

icantly higher expression in the RWV group than in the control group (Figure 2K).

Moreover, we investigated the ultrastructural organization of 3D-hiPSC-CTs by transmission electron microscopy and observed myofibrils, mitochondria, and cardiac desmosomes in both groups. However, in the RWV group, more mature myofibrils and cardiac desmosomes were detected, which were involved in wider sarcomeres, along with better-developed cardiac desmosomes (Figure 2L). These findings indicated that the RWV bioreactor facilitates the enhanced molecular and structural development and maturity of CMs in 3D-hiPSC-CTs.

### Dynamic culture in an RWV bioreactor enhances the motility of 3D-hiPSC-CTs

To evaluate the contractility of a 3D-hiPSC-CT, we performed motility analysis using a high-speed camera-based motion analysis system. Videos S1 and S2 depict the high-velocity area as red and the low-velocity area as blue. Contraction velocity ( $27.7 \pm 2.3$  versus  $15.3 \pm 1.0$   $\mu\text{m/s}$ ;  $p = 0.0011$ ;  $n = 5$  per group), relaxation velocity ( $15.7 \pm 1.5$  versus  $8.0 \pm 1.1$   $\mu\text{m/s}$ ;  $p = 0.0028$ ;  $n = 5$  per group), and acceleration ( $983 \pm 83$  versus  $623 \pm 26$   $\mu\text{m/s}^2$ ;  $p = 0.0033$ ;  $n = 5$  per group) were significantly higher in the RWV group than in the control group (Figures 3B–3D). Moreover, the contraction deformation distance ( $3.14 \pm 0.36$  versus  $1.70 \pm 0.20$   $\mu\text{m}$ ;  $p = 0.0079$ ;  $n = 5$  per group) and relaxation deformation distance ( $2.80 \pm 0.45$  versus  $1.44 \pm 0.26$   $\mu\text{m}$ ;  $p = 0.0309$ ;  $n = 5$  per group) were significantly longer in the RWV group than in the control group (Figures 3E–3F). Thus, the RWV bioreactor improved the 3D-hiPSC-CT motility.

Furthermore, we evaluated the change in motility of 3D-hiPSC-CTs in response to isoproterenol. In both groups, each parameter generally increased depending on the concentration of isoproterenol; however, at 100 and 1,000 nM, the rate of increase was significantly higher in the RWV group than in the control group ( $n = 10$  per group; Figures 3G–3K). These findings suggest that the RWV bioreactor improved the drug responsiveness of 3D-hiPSC-CTs.

(F–H) Representative immunostaining images of 3D-hiPSC-CTs.

(F) Green = collagen 4 (Col 4); (G) green = laminin (Lam); (H) red = fibronectin (Fib), blue = DAPI. Scale bar, 50  $\mu\text{m}$ . In the RWV group, fibronectin was expressed on both the upper and lower sides of a 3D-hiPSC-CTs.

(I) Representative western blots (WB) of TNT, SAA, CX43, MYH7, and GAPDH from 3D-hiPSC-CTs.

(J) Quantification of protein expression (mean  $\pm$  SE) from WB by densitometry, normalized to GAPDH, in the RWV and control groups ( $n = 5$  per group). Independent experiments, one-tailed Student's *t* test. \*\* $p < 0.01$  and \*\*\* $p < 0.001$ .

(K) qPCR of genes associated with ion channels (*SCN5A*, *CACNA1C*, *KCNJ2*, and *KCND3*), gap junctions (*CX43*), and myosin (*MLC2A*, *MLC2V*, *MYH6*, and *MYH7*) (mean  $\pm$  SE) in 3D-hiPSC-CTs from the RWV and control groups ( $n = 5$  per group). Independent experiments, one-tailed Student's *t* test. \* $p < 0.05$  and \*\* $p < 0.01$ .

(L) Representative transmission electron microscopy images of 3D-hiPSC-CTs. The yellow and white arrows indicate myofibrils and cardiac desmosomes, respectively. In the RWV group, wider myofibrils and better-developed cardiac desmosomes can be observed.

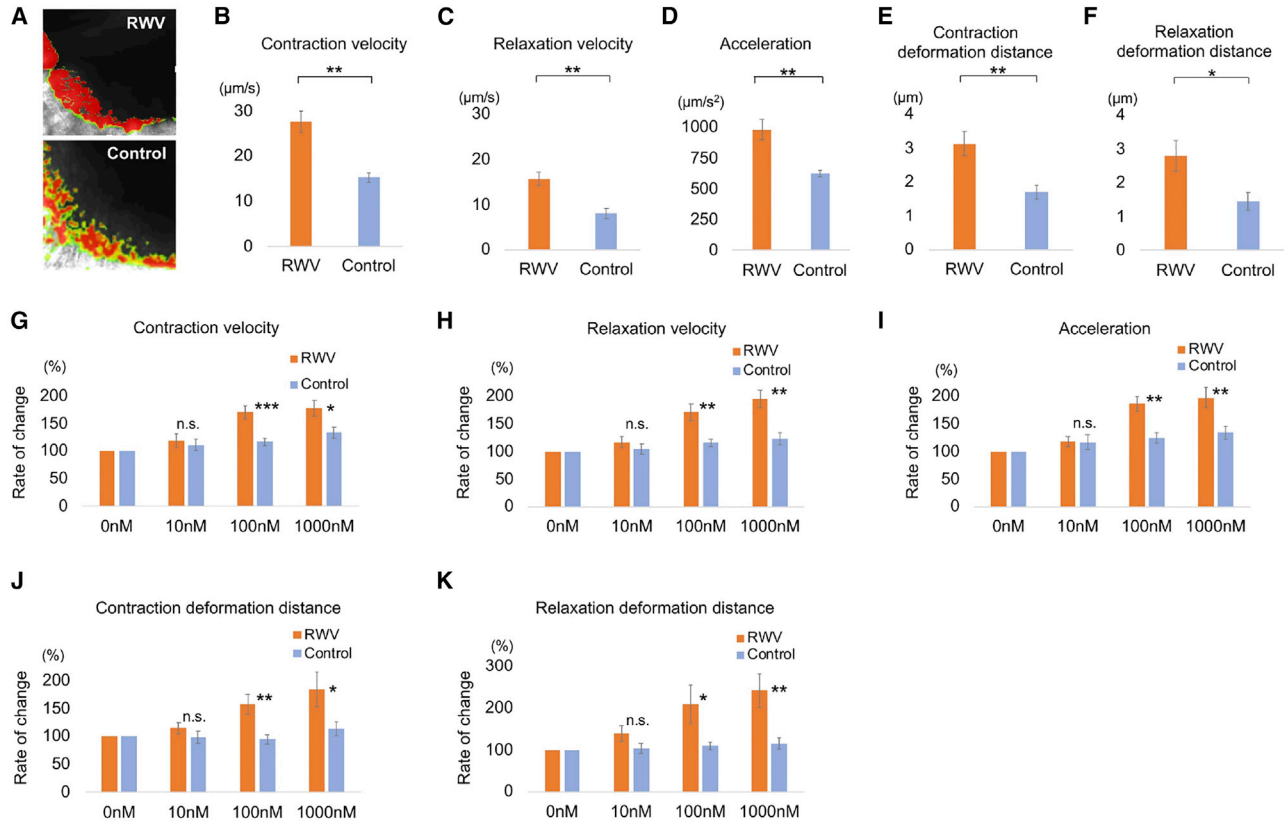


**Figure 3. Dynamic culture in a rotating wall vessel (RWV) bioreactor improves motility and drug responsiveness of a three-dimensional cardiac tissue derived from human-induced pluripotent stem cells (3D-hiPSC-CT)**

(A) Representative velocity data in RWV and control groups by a motion analysis system; red color represents high velocity. (B–F) Contractile properties of 3D-hiPSC-CT: contraction velocity (B), relaxation velocity (C), acceleration (D), contraction deformation distance (E), and relaxation deformation distance (F) (mean ± SE) in the RWV and control groups (n = 5 per group). \*p < 0.05 and \*\*p < 0.01.

(G–K) Contractile properties of 3D-hiPSC-CT in response to isoproterenol. Increased rate of contraction velocity (G), relaxation velocity (H), acceleration (I), contraction deformation distance (J), and relaxation deformation distance (K) (mean ± SE) at each concentration in the RWV and control groups (n = 10 per group). Independent experiments, one-tailed Student's *t* test. \*p < 0.05, \*\*p < 0.01, and \*\*\*p < 0.001. n.s., not significant.

### Dynamic culture in an RWV bioreactor promotes the electrophysiological development of a 3D-hiPSC-CT

To investigate the impact of the differential expression of Cx43 on the electrophysiological properties of 3D-hiPSC-CTs, we used a multielectrode array (MEA) data acquisition system. The signal amplitude ( $4,487 \pm 212$  versus  $1,088 \pm 93$  μV; p < 0.0001; n = 5 per group; Figure 4B) and conduction velocity ( $16.2 \pm 1.3$  versus  $10.2 \pm 1.0$  cm/s; p = 0.0070; n = 5 per group; Figure 4C) were significantly higher in the RWV group than in the control group. Thus, the RWV bioreactor improved the electrophysiological properties of the 3D-hiPSC-CT.

Dynamic culture in an RWV bioreactor increases the production of angiogenic cytokines and upregulates the mammalian target of rapamycin (mTOR) signaling pathway via integrin.

Next, we examined the mechanisms by which the RWV bioreactor affects 3D-hiPSC-CTs. To assess 3D-hiPSC-CT maturation mechanisms, we investigated the concentration of cytokines in culture supernatants derived from 3D-hiPSC-CTs by enzyme-linked immunosorbent assay (ELISA). The RWV group had higher vascular endothelial growth factor (VEGF;  $23.5 \pm 4.0$  versus  $7.8 \pm 1.2$  pg/mL; p = 0.0053; n = 5 per group) and hepatocyte growth factor (HGF;  $72.7 \pm 4.4$  versus  $41.2 \pm 3.8$  pg/mL; p = 0.0007; n = 5 per group) concentrations than those of the control group (Figures 5A and 5B). Therefore, the RWV bioreactor was considered to promote vasculature formation.

Additionally, we used western blotting to investigate the signaling pathways involved in the maturation of 3D-hiPSC-CTs. Specifically, we evaluated the activation of integrin α7, integrin β1, and focal adhesion kinase (FAK),

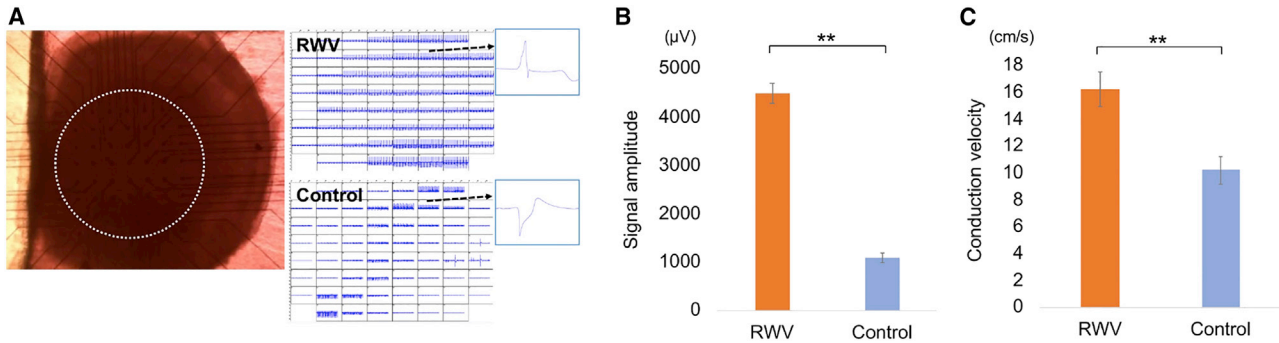


**Figure 4. Dynamic culture in a rotating wall vessel (RWV) bioreactor promotes electrophysiological development of a three-dimensional cardiac tissue derived from human-induced pluripotent stem cells (3D-hiPSC-CT)**

(A) Images of 3D-hiPSC-CT analyzed with the multielectrode array data acquisition system and electrical signals recorded by electrodes. The white dotted area indicates the electrodes.

(B) Signal voltage (peak to peak amplitude) (mean  $\pm$  SE) of 3D-hiPSC-CTs in the RWV and control groups (n = 5 per group). Independent experiments, one-tailed Student's *t* test. \*\**p* < 0.01.

(C) Conduction velocity of 3D-hiPSC-CTs (mean  $\pm$  SE) in the RWV and control groups (n = 5 per group). Independent experiments, one-tailed Student's *t* test. \*\**p* < 0.01.

which are expressed in CMs and activated by mechanical stress, such as shear stress. In the RWV group, integrin  $\alpha 7$  ( $1.5 \pm 0.1$  versus  $1.0 \pm 0.04$ ; *p* = 0.0098; n = 5 per group), integrin  $\beta 1$  ( $2.0 \pm 0.1$  versus  $1.0 \pm 0.1$ ; *p* < 0.0001; n = 5 per group), and the ratio of phosphorylated to total FAK (phosphorylated/total:  $2.2 \pm 0.3$  versus  $1.0 \pm 0.1$ ; *p* = 0.0028; n = 5 per group) showed significantly higher expression than those of the control group (Figures 5C and 5D). Activation of mTOR signaling, which is a mechanical stress-related mediator related to cell growth and protein synthesis, was also evaluated. In the RWV group, the ratios of phosphorylated to total mTOR (phosphorylated/total:  $2.2 \pm 0.1$  versus  $1.0 \pm 0.1$ ; *p* = 0.0003; n = 5 per group) and S6K (phosphorylated/total:  $3.2 \pm 0.4$  versus  $1.0 \pm 0.1$ ; *p* = 0.0012; n = 5 per group) were significantly higher than those of the control group (Figures 5C and 5D). We also investigated the activation of protein kinase B (AKT), which is one of the upstream regulators of mTOR and one of the downstream effectors of FAK; however, no significant difference was observed in the ratio of phosphorylated to total AKT between the RWV and control groups (phosphorylated/total:  $0.9 \pm 0.1$  versus  $1.0 \pm 0.04$ ; *p* = 0.1834; n = 5 per group; Figures 5C and 5D). These results suggested that the mTOR signaling pathway may be involved in the mechanism of 3D-hiPSC-CT maturation.

### 3D-hiPSC-CTs cultured in an RWV bioreactor present enhanced therapeutic effects *in vivo*

We then transplanted 3D-hiPSC-CTs into the hearts of a nude rat MI model. Four weeks later, 3D-hiPSC-CTs of the RWV group survived in seven out of 10 rats, as evident in immunohistochemical images; however, in the control group, survival of 3D-hiPSC-CTs was only

observed in three out of the 10 rats. In the transplanted tissues, vascular-like structures, double-stained with isolectin B4 and SMA, were partially observed (Figures 6A–6D). As shown in Figures 6E–6G, the RWV group rats exhibited a significantly higher LV ejection fraction (LVEF;  $46.1\% \pm 1.7\%$ ) than that of the control group ( $40.4\% \pm 0.6\%$ ; *p* = 0.0032) and sham rats ( $36.4\% \pm 0.7\%$ ; *p* < 0.0001) at 1 week [ANOVA: *p* < 0.0001; n = 10 per group], 2 weeks (RWV  $48.0\% \pm 1.2\%$  versus control  $40.8\% \pm 1.5\%$  [*p* = 0.0014] versus sham  $35.9\% \pm 1.0\%$  [*p* < 0.0001]; ANOVA *p* < 0.0001; n = 10 per group), 3 weeks (RWV  $48.9\% \pm 1.7\%$  versus control  $40.6\% \pm 1.9\%$  [*p* = 0.0034] versus sham  $35.0\% \pm 1.1\%$  [*p* < 0.0001]; ANOVA: *p* < 0.0001; n = 10 per group), and 4 weeks (RWV  $47.0\% \pm 1.6\%$  versus control  $37.6\% \pm 2.2\%$  [*p* = 0.0018] versus sham  $32.3\% \pm 1.3\%$  [*p* < 0.0001]; ANOVA *p* < 0.0001; n = 10 per group) after transplantation. Regarding the LV dimensions, the LV end-diastolic dimension (LVDd) in the RWV group was significantly smaller than that in the sham rats at 3 weeks ( $8.08 \pm 0.19$  mm versus  $8.71 \pm 0.13$  mm, *p* = 0.0252; ANOVA: *p* = 0.0317; n = 10 per group) and 4 weeks ( $8.11 \pm 0.19$  mm versus  $8.89 \pm 0.14$  mm, *p* = 0.0070; ANOVA: *p* = 0.0093; n = 10 per group) after transplantation. Moreover, the LV end-systolic dimension (LVDs) in the RWV group was significantly smaller than in the control group and sham rats at 2 weeks (RWV  $6.30 \pm 0.12$  mm versus control  $6.91 \pm 0.17$  mm [*p* = 0.0168] versus sham  $7.24 \pm 0.13$  mm [*p* = 0.0003]; ANOVA: *p* = 0.0003; n = 10 per group), 3 weeks (RWV  $6.33 \pm 0.15$  mm versus control  $7.00 \pm 0.16$  mm [*p* = 0.0104] versus sham  $7.44 \pm 0.14$  mm [*p* < 0.0001]; ANOVA: *p* < 0.0001; n = 10 per group), and 4 weeks (RWV  $6.44 \pm 0.16$  mm versus control

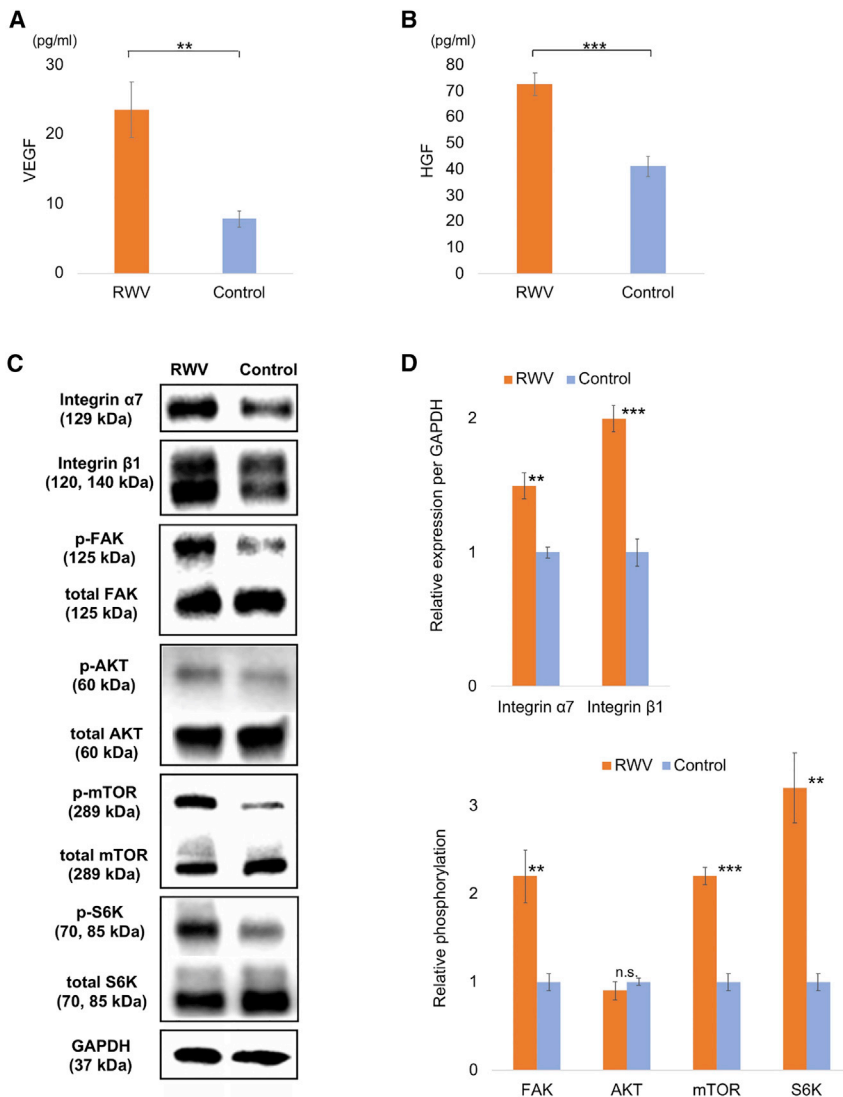


**Figure 5. Dynamic culture in a rotating wall vessel (RWV) bioreactor promotes production of angiogenic cytokines from a three-dimensional cardiac tissue derived from human-induced pluripotent stem cells (3D-hiPSC-CT), and it upregulates the mammalian target of rapamycin (mTOR) signaling pathway via integrin**

(A and B) Concentrations of vascular endothelial growth factor (VEGF) (A) and hepatocyte growth factor (HGF) (B) (mean  $\pm$  SE) in the culture supernatant of RWV and control groups ( $n = 5$  per group). Independent experiments, one-tailed Student's  $t$  test. \*\* $p < 0.01$  and \*\*\* $p < 0.001$ .

(C) Representative western blots (WB) for integrin  $\alpha 7$ , integrin  $\beta 1$ , phosphorylated and total focal adhesion kinase (FAK), phosphorylated and total AKT, phosphorylated and total mTOR, phosphorylated and total S6K, and GAPDH from 3D-hiPSC-CTs.

(D) Quantification of protein expression (mean  $\pm$  SE) from WB by densitometry, normalized to GAPDH, and the quantified ratio of phosphorylated/total protein for each kinase in (C) normalized to those of the control group ( $n = 5$  per group). Independent experiments, one-tailed Student's  $t$  test. \*\* $p < 0.01$  and \*\*\* $p < 0.001$ . n.s., not significant.

$7.21 \pm 0.15$  mm [ $p = 0.0046$ ] versus sham  $7.72 \pm 0.16$  mm [ $p < 0.0001$ ]; ANOVA:  $p < 0.0001$ ;  $n = 10$  per group) after transplantation. Additionally, in the RWV group, the fibrotic area in the recipient myocardium ( $17.0\% \pm 1.4\%$ ), which was associated with LV remodeling and exhibited extracellular collagen deposition, was smaller than that in the control group ( $24.2\% \pm 1.6\%$ ;  $p = 0.0035$ ) and the sham group ( $33.8\% \pm 1.1\%$ ;  $p < 0.0001$ ; ANOVA:  $p < 0.0001$ ;  $n = 10$  per group; **Figure 6H**). Regarding cardiomyocyte hypertrophy at an area remote from the infarct, the average diameter of cardiomyocytes in the RWV group rats ( $16.3 \pm 0.54$   $\mu$ m) was smaller than that in the control group ( $18.2 \pm 0.65$   $\mu$ m;  $p = 0.0664$ ) and sham group ( $20.8 \pm 0.60$   $\mu$ m;  $p < 0.0001$ ; ANOVA:  $p < 0.0001$ ;  $n = 10$  per group; **Figure 6I** and **Figure S3**). Moreover, in the RWV group, the capillary density

( $545 \pm 36/\text{mm}^2$ ), which is related to neovascularization, was higher than that in the control group ( $356 \pm 29/\text{mm}^2$ ;  $p = 0.0002$ ) and sham group ( $224 \pm 17/\text{mm}^2$ ;  $p < 0.0001$ ; ANOVA:  $p < 0.0001$ ;  $n = 10$  per group; **Figure 6J**).

Quantitative reverse transcriptase PCR (qRT-PCR) analysis revealed that the expression levels of *VEGF* and *HGF* were significantly higher in the RWV group rats than in the sham rats (*VEGF*:  $1.5 \pm 0.2$  versus  $1.0 \pm 0.04$ ;  $p = 0.0342$ ;  $n = 8$  per group; **Figure 6K**, *HGF*:  $2.1 \pm 0.3$  versus  $1.0 \pm 0.1$ ;  $p = 0.0066$ ;  $n = 8$  per group; **Figure 6L**, respectively). However, the expression levels of *VEGF* and *HGF* were only slightly and not significantly higher in the RWV group compared with those of the controls (*VEGF*:  $1.5 \pm 0.2$  versus  $1.2 \pm 0.06$ ;  $p = 0.1572$ ;  $n = 8$  per group; **Figure 6K**, *HGF*:  $2.1 \pm 0.3$  versus  $1.7 \pm 0.2$ ;  $p = 0.3651$ ;  $n = 8$  per group; **Figure 6L**, respectively).

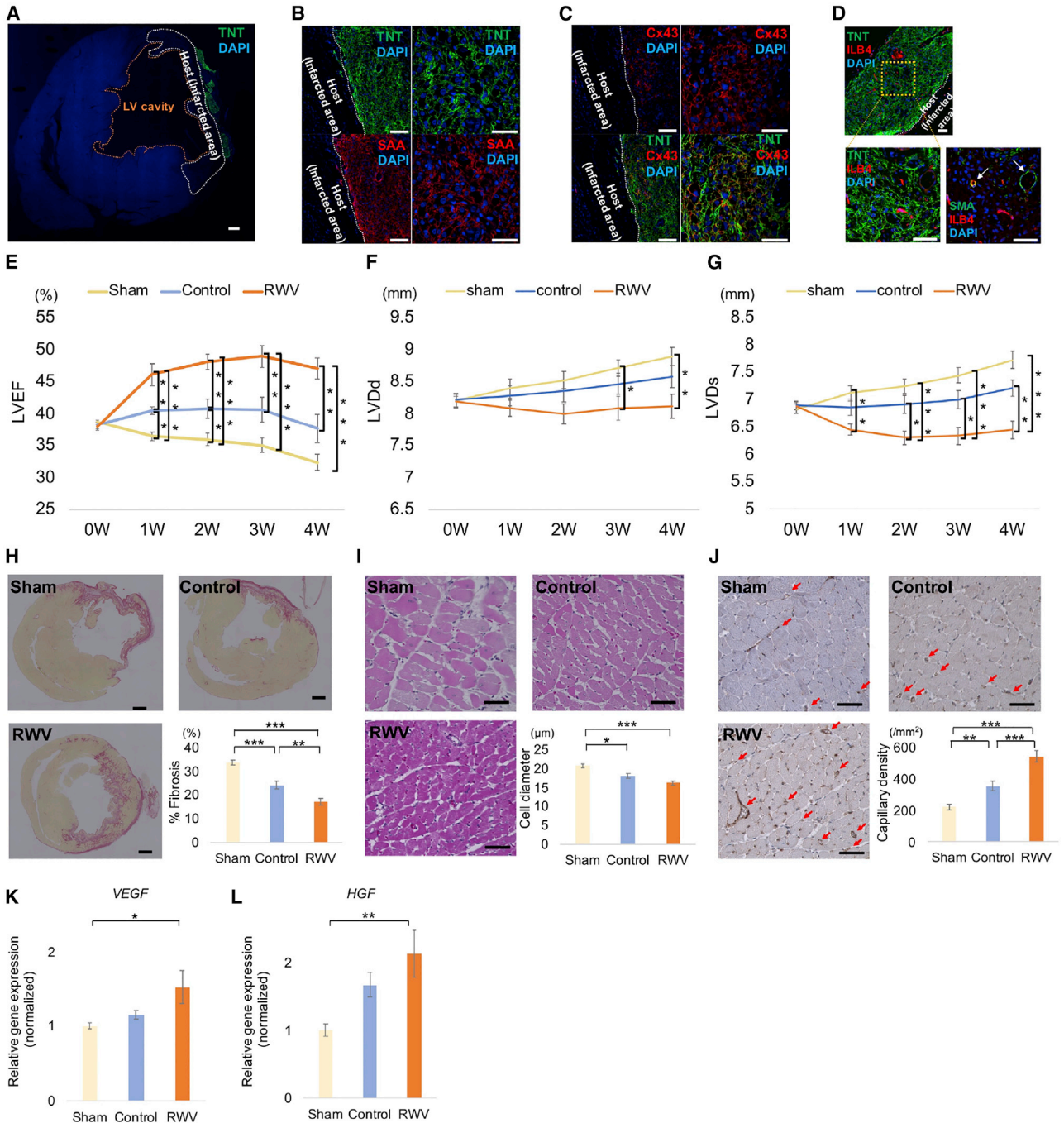


**Figure 6. A three-dimensional cardiac tissue derived from human-induced pluripotent stem cells (3D-hiPSC-CT), cultured in rotating wall vessel (RWV) bioreactor, enhances therapeutic effects *in vivo***

(A–D) Representative immunostained images of 3D-hiPSC-CTs transplanted into a rat myocardial infarction model in the RWV group (4 weeks after transplantation). (A) Full image, green = human troponin T (TNT); scale bar, 500 μm; (B) magnified images, red = sarcomeric α actinin (SAA); (C) red = connexin 43 (CX43); scale bar, 100 μm (left), 50 μm (right); (D) red = isolectin B4 (ILB4), green = TNT (top) (left, bottom), green = smooth muscle actin (right, bottom), blue = DAPI; scale bar, 100 μm (top), 50 μm (bottom). In the RWV group, the thickness of the 3D-hiPSC-CT was >500 μm 4 weeks after transplantation, and mature vessels were observed within (white arrows).

(legend continued on next page)



These findings collectively suggest that 3D-hiPSC-CTs cultured in an RWV bioreactor could facilitate engraftment with vasculature formation in diseased recipient hearts, and thereby improve cardiac function while preventing LV reverse remodeling.

## DISCUSSION

The primary findings of this study are as follows. First, dynamic culture in an RWV bioreactor was found to facilitate the maturation of 3D-hiPSC-CTs morphologically, mechanically, and electrophysiologically. This conclusion was supported by the following results. Dynamic culture in an RWV bioreactor allowed 3D-hiPSC-CTs to acquire the following: (1) increased thickness along with growth of cardiomyocytes; (2) increased expression of sarcomeric proteins (TNT, SAA, MYH7) and a gap junction protein (CX43); (3) massive myofibrils with A-, H-, and I-bands, and cardiac desmosome with integrity; (4) improved contraction and relaxation abilities; (5) increased field potential and accelerated conduction velocity; and (6) improved drug responsiveness. Moreover, in the *in vivo* rat model of MI, those transplanted with 3D-hiPSC-CTs cultured in an RWV bioreactor showed improved engraftment in the infarct region as well as superior cardiac function with prevention of LV reverse remodeling compared with the effects of transplanted 3D-hiPSC-CTs that were cultured under static condition.

Mature CTs may offer certain advantages during cardiomyogenesis in a severely damaged myocardium, since they exhibit specific unique features such as (1) higher expression of sarcomeric proteins, as well as a thicker and longer sarcomere structure, resulting in improved contractile properties (Germanguz et al., 2011; Lundy et al., 2013; Zhang et al., 2009); (2) higher action potential, expression of gap junction proteins, such as Cx43, and polarity, result-

ing in increased conduction velocity and electrical stability (Gao et al., 2018; Ribeiro et al., 2015; Yang et al., 2014); and (3) greater secretion of angiogenic cytokines (Yoshida et al., 2018). Therefore, establishing means for developing matured cardiac tissue *ex vivo* would be crucial for ameliorating a severely damaged heart with few remaining viable myocytes.

In this study, we demonstrated the development of mature CTs with higher expression of contractile and gap junction proteins due to the application of fluid shear stress. We then hypothesized the possible involvement of the integrin-FAK-AKT-mTOR signaling pathway in the maturation mechanism (by dynamic culture) occurring in an RWV bioreactor (Figure S4). Specifically, integrin exhibits mechano-sensing functions with its expression increasing upon mechanical stimulation, such as stretch or shear stress. Integrin also regulates the activity of FAK (Boppart and Mahmassani, 2019; Israeli-Rosenberg et al., 2014; Lorenz et al., 2018; Urbich et al., 2000), which in turn regulates AKT and mTOR signaling and controls various cellular activities, such as survival, adhesion, and proliferation (Jindra et al., 2008; Nguyen et al., 2018; Xia et al., 2004; You et al., 2015). In the heart, the mTOR signaling pathway is involved in the regulation of embryonic cardiovascular development, control of intracellular processes related to normal postnatal growth and maintenance of cardiac function, as well as activation of mTOR complex 1 (mTORC1), followed by that of S6K, thereby promoting protein synthesis (Kemi et al., 2008; Laplante and Sabatini, 2012; Sciarretta et al., 2014). In our study, 3D-hiPSC-CTs cultured in an RWV bioreactor had higher activities of integrin-FAK and mTOR pathway signaling compared with those grown under static conditions. However, no significant difference was observed in AKT activity between the RWV and control groups. This may have been caused by the negative feedback regulation from S6K, which is observed in the chronic phase of dynamic culture

(E–G) Changes in left ventricular ejection fraction (LVEF) (E), left ventricular end-diastolic dimension (LVDD) (F), and left ventricular end-systolic dimension (LVSD) (G) (mean  $\pm$  SE) in each group after transplantation, analyzed by transthoracic echocardiography (n = 10 per group). Independent experiments, one-way ANOVA followed by the post-hoc Tukey HSD test. \*p < 0.05, \*\*p < 0.01, and \*\*\*p < 0.001. (H) Representative images of myocardial fibrosis in each group, as assessed by Sirius Red staining. Scale bar, 1,000  $\mu$ m. The right bottom graph shows the percentage of fibrotic (mean  $\pm$  SE) to myocardial tissue in each group (n = 10 per group). Independent experiments, one-way ANOVA followed by the post-hoc Tukey HSD test. \*\*p < 0.01, and \*\*\*p < 0.001.

(I) Representative images of cardiomyocytes at an area remote from the infarct in each group, as assessed by hematoxylin and eosin staining. Scale bar, 1,000  $\mu$ m. The right bottom graph shows the diameter of cardiomyocyte (mean  $\pm$  SE) in each group (n = 10 per group, average diameter of 10 cardiomyocytes randomly selected from one image). Independent experiments, one-way ANOVA followed by the post-hoc Tukey HSD test. \*p < 0.05, and \*\*\*p < 0.001.

(J) Representative immunostained images of vWF in each group. Scale bar, 50  $\mu$ m. The red arrows indicate the capillary vessels. The right bottom graph shows the capillary density per unit area (mean  $\pm$  SE) in each group (n = 10 per group). Independent experiments, one-way ANOVA followed by the post-hoc Tukey HSD test. \*\*p < 0.01 and \*\*\*p < 0.001.

(H–I) Expression of vascular endothelial growth factor (VEGF) (K) and hepatocyte growth factor (HGF) (L) genes (mean  $\pm$  SE) in each group, normalized against GAPDH expression (n = 8 per group). Independent experiments, one-way ANOVA followed by the post-hoc Tukey HSD test. \*p < 0.05 and \*\*p < 0.01.



(Jackman et al., 2016). In addition, there might be a signaling pathway other than the integrin-FAK-AKT-mTOR pathway that activates mTOR from integrin without the involvement of AKT.

We also observed that dynamic culture in an RWV bioreactor enhanced the engraftment and therapeutic effect of 3D-hiPSC-CTs in a failed heart in the MI rat model. The following two factors might be strongly involved in the enhanced engraftment effect. First, 3D-hiPSC-CTs cultured in an RWV bioreactor secreted higher levels of angiogenic cytokines due to the promoted maturation of cardiomyocytes. Second, the high secretion of angiogenic cytokines not only promoted angiogenesis in the transplanted tissues but also promoted the induction of mature blood vessels from the recipient heart into the transplanted tissues. These factors may facilitate adequate oxygen and nutrient supply to the transplanted tissues over an extended period of time, resulting in improved engraftment. In fact, the transplanted tissues survived for 1 month in seven of the 10 rats in the RWV group compared to only three of the 10 control rats. To further improve engraftment, combining the current method with a process to cover transplanted tissues with an omental flap containing a rich vascular network may be necessary (Kawamura et al., 2013, 2017).

We also observed significant differences in the fibrotic area, the diameter of cardiomyocyte, capillary density, and angiogenic cytokine expression across the three groups. Therefore, reduced LV remodeling caused by a paracrine effect may be one of the mechanisms associated with enhanced therapeutic effects on the diseased rat heart, as demonstrated in previous reports (Kawamura et al., 2012, 2013, 2017; Weinberger et al., 2016; Wendel et al., 2015; Yoshida et al., 2018). However, it remains to be determined whether transplanted tissues are capable of assisting the recipient tissue in dynamic beating. In the RWV group, expression levels of contractile proteins were higher than those of controls, and the thickness of the transplanted tissues reached 500–1,000  $\mu\text{m}$  in the recipient infarcted region, thereby suggesting that transplanted tissues have certain potential in providing pulsatile support.

If 3D-hiPSC-CTs are constructed for human application, it is estimated that approximately  $8 \times 10^8$  cells would be required for a human weighing 60 kg based on our results. Assuming that a 3D-hiPSC-CT with the same thickness as that used in this study can be engineered, and if the area is multiplied by 200, three 3D-hiPSC-CTs of  $50 \times 50$  mm will be required. The size of the RWV could be tailored according to the size of the 3D-hiPSC-CT.

Further maturation of 3D-hiPSC-CTs might be possible by adding an electrical stimulator or stretching function to this bioreactor, but the device may then become complicated. We believe that the RWV bioreactor is the best

option for clinical use at present owing to the ease of management.

In conclusion, dynamic culture in an RWV bioreactor promotes the *ex vivo* maturation of 3D-hiPSC-CTs by enhancing the cardiogenic potential and assisting functional recovery with improved engraftment in a diseased heart. Hence, this platform has potential for promoting cardiomyogenesis for cases of severe heart failure.

## EXPERIMENTAL PROCEDURES

Expanded experimental procedures performed in this study are available in the online [supplemental information](#), including details of ELISAs, qRT-PCR, western blotting, histology, transmission electron microscopy, and echocardiography. All procedures and protocols involving animals were approved by the ethics committee of Osaka University (approval number: 01-062-000) and were performed according to the committee's guidelines. All animal experiments complied with the ARRIVE guidelines and were carried out in accordance with the National Institutes of Health Guide for the Care and Use of Laboratory Animals (NIH Publications No. 8023, revised 1978).

### Cardiac differentiation of hiPSCs

Human-induced pluripotent stem cells (hiPSCs; 253G1; Riken, Ibaraki, Japan) were used in this study. Undifferentiated hiPSCs were cultured and maintained in primate embryonic stem cell medium (ReproCELL, Kanagawa, Japan) with 5 ng/mL basic fibroblast growth factor (bFGF; ReproCELL) on mitomycin C-treated mouse embryonic fibroblast cells (ReproCELL). Cardiomyogenic differentiation was induced as previously described with specific modifications (Matsuura et al., 2012). Briefly, cardiac differentiation was induced in StemPro 34 medium (Thermo Fisher Scientific, Waltham, MA, USA) containing 2 mM L-glutamine (Thermo Fisher Scientific), 50  $\mu\text{g}/\text{mL}$  ascorbic acid (FUJIFILM Wako Pure Chemical Corporation, Osaka, Japan), and 400  $\mu\text{M}$  1-thioglycerol (Sigma-Aldrich, St. Louis, MO, USA). The medium was also supplemented with several human recombinant proteins, including bone morphologic protein 4, activin A, bFGF (R&D Systems, Minneapolis, MN, USA), and VEGF (FUJIFILM Wako Pure Chemical Corporation), and small molecules, including IWR-1 and IWP-2 (Sigma-Aldrich). hiPSCs were dissociated using Accumax (Nacalai Tesque, Kyoto, Japan) and transferred to a bioreactor (ABLE Corporation & Biott, Tokyo, Japan). hiPSC-CMs were maintained in Dulbecco's modified Eagle's medium (DMEM; Nacalai Tesque) supplemented with 10% fetal bovine serum (FBS; Sigma-Aldrich).

### Construction of 3D-hiPSC-CTs and culture in an RWV bioreactor

We engineered the 3DCT by seeding hiPSC-derived CMs on a poly(lactic-co-glycolic acid) fiber sheet (3D-hiPSC-CT), as described previously (Li et al., 2017). The process from construction of the 3D-hiPSC-CT to culture in an RWV bioreactor is outlined in [Figure S5](#). In brief, a cell suspension was prepared, including  $2.0 \times 10^6$  cells per 60  $\mu\text{L}$  of DMEM (Nacalai Tesque) with 10% FBS (Sigma-Aldrich), 50 units/mL penicillin, and 50  $\mu\text{g}/\text{mL}$



streptomycin (Thermo Fisher Scientific). Furthermore,  $1.0 \times 10^{-5}$   $\mu\text{g}/\text{mL}$  recombinant human laminin511-E8 fragments (MATR IXOME, Osaka, Japan) and  $10 \mu\text{M}$  Y-27632 (Nacalai Tesque) were added to the cell suspension. The suspension was then seeded on a 6-mm square poly(lactic-co-glycolic acid) aligned fiber sheet at  $60 \mu\text{L}$  per sheet (3D-hiPSC-CT). Three hours after seeding,  $5 \text{ mL}$  of culture medium was added per sheet. After incubating the 3D-hiPSC-CT under static conditions for 3 days, it was transferred to an RWV bioreactor (JTEC Corporation, Osaka, Japan) (Figure S6) and cultured for an additional 7 days (RWV group). The rotation speed was  $10 \text{ rpm}$  to maintain the 3D-hiPSC-CT afloat in the RWV bioreactor (Video S3). The control group continued the culture under static conditions for an additional 7 days. The volume of the culture medium was  $50 \text{ mL}$  for both groups.

### Cell viability assay

Cell viability was evaluated using LIVE/DEAD Viability/Cytotoxicity Kit (Thermo Fisher Scientific). In brief,  $4 \mu\text{M}$  ethidium homodimer solution and  $2 \mu\text{M}$  Calcein AM were prepared and mixed to form a working solution. This solution was added directly to the 3D-hiPSC-CTs. After incubation for 30–45 min at  $37^\circ\text{C}$ , the tissues were assessed using confocal microscopy (FLUOVIEW FV10i; Olympus, Tokyo, Japan). Nuclei of the dead cells are stained red, whereas those of live cells are stained green. The numbers of live and dead cells were then counted in nine different areas per sample, and the average represented the viable cell percentage.

### Cell motility analysis

The beating of 3D-hiPSC-CTs was monitored at 150 frames per second, a resolution of  $512 \times 512$  pixels, and a depth of 8 bits for 10 s at  $37^\circ\text{C}$  using a high-speed camera-based motion analysis system (SI8000 view software; Sony, Tokyo, Japan). The beating rate, contraction velocity, relaxation velocity, acceleration, contraction deformation distance, and relaxation deformation distance were measured using SI8000C analyzer software (Sony). To evaluate drug loading, 10, 100, or 1,000 nM isoproterenol (Sigma-Aldrich) was added to the culture medium, and the motion of 3D-hiPSC-CTs was monitored, recorded, and assessed.

### Electrophysiological characterization

Extracellular field potentials (FPs) of 3D-hiPSC-CTs were determined using the MEA data acquisition system (USB-ME64-System; Multi Channel Systems, BW, Germany). Signals were recorded on day 10 after plating the hiPSC-CMs. An isochronal map was created based on linear interpolation between the electrodes (Meiry et al., 2001) and calculated using the MATLAB function (MATLAB; MathWorks, Natick, MA, USA). The amplitude and conduction velocity were determined by analyzing the wave forms of FPs.

### In vivo transplantation in a rat model of chronic MI

We generated the rat model of chronic MI, as described previously (Sekiya et al., 2009). Specifically, 8-week-old male nude rats (F344/NJcl-rnu/rnu; CLEA Japan, Tokyo, Japan) were anesthetized by isoflurane inhalation (2%,  $0.2 \text{ mL}/\text{min}$ ), intubated, and placed on a respirator during surgery to maintain ventilation. Thoracotomy was performed between the fourth and fifth intercostal spaces,

and MI was induced by ligation of the left coronary artery. Two weeks after left coronary artery ligation, transthoracic echocardiography was performed to validate the extent of MI. Since we aimed to create a model of widespread MI, rats with an ejection fraction greater than 45% were excluded. These models were randomly divided into three treatment groups ( $n = 10$  per group): (1) transplantation of 3D-hiPSC-CT cultured in an RWV bioreactor (RWV group), (2) transplantation of 3D-hiPSC-CT cultured under static conditions (control group), and (3) sham operation (sham group). For transplantation, thoracotomy was again performed between the fourth and fifth intercostal spaces, and the pericardium was peeled back to identify the infarct area. For animals in the 3D-hiPSC-CT group, two 3D-hiPSC-CTs were transplanted into each heart. After cutting out the polydimethylsiloxane frame of 3D-hiPSC-CTs, they were placed directly onto the infarct area, which was then covered with Beriplast P (CSL Behring, King of Prussia, PA, USA) and the pericardium to prevent their slipping off of the infarct area. Four weeks after transplantation, the rats were sacrificed through an anesthetic overdose and the hearts were removed. Engraftment of transplanted 3D-hiPSC-CTs was evaluated by immunostaining of a middle ventricular cross-section image immunostaining with a human cTnT. The fibrotic area in the recipient myocardium was evaluated by a middle ventricular cross-section image stained with Sirius Red and calculated with MetaMorph Microscopy Automation & Image Analysis Software (Molecular Devices, San Jose, CA, USA). The diameters of the recipient cardiomyocytes were measured at an area remote from the infarct in a middle ventricular cross-section image stained with H&E. Ten recipient cardiomyocytes per sample were measured and then averaged. The capillary density was measured at the infarct border zone in a middle ventricular cross-section image immunostained with von Willebrand factor (vWF). The number of vessels stained with vWF was counted at five areas in the infarct border zone per sample and averaged.

### Statistics

Continuous variables are summarized as the mean  $\pm$  SE of the mean. Differences between two groups were analyzed by one-tailed Student's *t* test. Comparisons tests across multiple groups were analyzed by one-way ANOVA followed by the post-hoc Tukey HSD test. Statistical significance was defined as  $p < 0.05$ . All data were analyzed using JMP Pro 14 (SAS Institute, Cary, NC, USA).

### SUPPLEMENTAL INFORMATION

Supplemental information can be found online at <https://doi.org/10.1016/j.stemcr.2022.03.012>.

### AUTHOR CONTRIBUTIONS

T. N., S. M., T. U., L. L., and Y. S. conceived the project. T. N., S. M., and T. K. designed the experiments. T. N. and J. L. performed experiments. All authors contributed to data analysis and interpretation. T. N., S. M., and T. K. wrote the manuscript.

### CONFLICTS OF INTERESTS

JTEC Corporation provided support in the form of salary for Toshimasa Uemura but did not have any additional role in the study



design, data collection and analysis, decision to publish, or preparation of the manuscript. The other authors declare no competing interests. Two patents are related to this work. First, the patent number is US20120083029. Second, the patent number is PCT/JP2015/079364.

## ACKNOWLEDGMENTS

We thank Nagako Sougawa, Maki Takeda, Seiko Eiraku, and Yuri Ide for their technical support during analysis. We also thank Yo Uemura, Meihua Jin, Kenichi Morita, and Takashi Tsumura for technical support with the RWV bioreactor. This work was supported by Grants-in-Aid for Scientific Research (KAKENHI, grant number 19K18179).

Received: January 29, 2021  
 Revised: March 19, 2022  
 Accepted: March 21, 2022  
 Published: April 14, 2022

## REFERENCES

Boppart, M.D., and Mahmassani, Z.S. (2019). Integrin signaling: linking mechanical stimulation to skeletal muscle hypertrophy. *Am. J. Physiol. Cell Physiol.* *317*, C629–C641. <https://doi.org/10.1152/ajpcell.00009.2019>.

Dvir, T., Levy, O., Shachar, M., Granot, Y., and Cohen, S. (2007). Activation of the ERK1/2 cascade via pulsatile interstitial fluid flow promotes cardiac tissue assembly. *Tissue Eng.* *13*, 2185–2193. <https://doi.org/10.1089/ten.2006.0364>.

Gao, L., Gregorich, Z.R., Zhu, W., Mattapally, S., Oduk, Y., Lou, X., Kannappan, R., Borovjagin, A.V., Walcott, G.P., Pollard, A.E., et al. (2018). Large cardiac muscle patches engineered from human induced-pluripotent stem cell-derived cardiac cells improve recovery from myocardial infarction in swine. *Circulation* *137*, 1712–1730. <https://doi.org/10.1161/CIRCULATIONAHA.117.030785>.

Germanguz, I., Sedan, O., Zeevi-Levin, N., Shtrichman, R., Barak, E., Ziskind, A., Eliyahu, S., Meiry, G., Amit, M., Itskovitz-Eldor, J., et al. (2011). Molecular characterization and functional properties of cardiomyocytes derived from human inducible pluripotent stem cells. *J. Cell. Mol. Med.* *15*, 38–51. <https://doi.org/10.1111/j.1582-4934.2009.00996.x>.

Godier-Furnémont, A.F., Tiburcy, M., Wagner, E., Dewenter, M., Lämle, S., El-Armouche, A., Lehnart, S.E., Vunjak-Novakovic, G., and Zimmermann, W.H. (2015). Physiologic force-frequency response in engineered heart muscle by electromechanical stimulation. *Biomaterials* *60*, 82–91. <https://doi.org/10.1016/j.biomaterials.2015.03.055>.

Imboden, M., de Coulon, E., Poulin, A., Dellenbach, C., Rosset, S., Shea, H., and Rohr, S. (2019). High-speed mechano-active multi-electrode array for investigating rapid stretch effects on cardiac tissue. *Nat. Commun.* *10*, 834. <https://doi.org/10.1038/s41467-019-08757-2>.

Israeli-Rosenberg, S., Manso, A.M., Okada, H., and Ross, R.S. (2014). Integrins and integrin-associated proteins in the cardiac myocyte. *Circ. Res.* *114*, 572–586. <https://doi.org/10.1161/CIRCRESAHA.114.301275>.

Jackman, C.P., Carlson, A.L., and Bursac, N. (2016). Dynamic culture yields engineered myocardium with near-adult functional output. *Biomaterials* *111*, 66–79. <https://doi.org/10.1016/j.biomaterials.2016.09.024>.

Jindra, P.T., Jin, Y.-P., Rozengurt, E., and Reed, E.F. (2008). HLA class I antibody-mediated endothelial cell proliferation via the mTOR pathway. *J. Immunol.* *180*, 2357–2366. <https://doi.org/10.4049/jimmunol.180.4.2357>.

Kawamura, M., Miyagawa, S., Miki, K., Saito, A., Fukushima, S., Higuchi, T., Kawamura, T., Kuratani, T., Daimon, T., Shimizu, T., et al. (2012). Feasibility, safety, and therapeutic efficacy of human induced pluripotent stem cell-derived cardiomyocyte sheets in a porcine ischemic cardiomyopathy model. *Circulation* *126*, S29–S37. <https://doi.org/10.1161/CIRCULATIONAHA.111.084343>.

Kawamura, M., Miyagawa, S., Fukushima, S., Saito, A., Miki, K., Ito, E., Sougawa, N., Kawamura, T., Daimon, T., Shimizu, T., et al. (2013). Enhanced survival of transplanted human induced pluripotent stem cell-derived cardiomyocytes by the combination of cell sheets with the pedicled omental flap technique in a porcine heart. *Circulation* *128*, S87–S94. <https://doi.org/10.1161/CIRCULATIONAHA.112.000366>.

Kawamura, M., Miyagawa, S., Fukushima, S., Saito, A., Miki, K., Funakoshi, S., Yoshida, Y., Yamanaka, S., Shimizu, T., Okano, T., et al. (2017). Enhanced therapeutic effects of human iPS cell derived-cardiomyocyte by combined cell-sheets with omental flap technique in porcine ischemic cardiomyopathy model. *Sci. Rep.* *7*, 8824. <https://doi.org/10.1038/s41598-017-08869-z>.

Kemi, O.J., Ceci, M., Wisloff, U., Grimaldi, S., Gallo, P., Smith, G.L., Condorelli, G., and Ellingsen, O. (2008). Activation or inactivation of cardiac AKT/mTOR signaling diverges physiological from pathological hypertrophy. *J. Cell. Physiol.* *214*, 316–321. <https://doi.org/10.1002/jcp.21197>.

Laplanche, M., and Sabatini, D.M. (2012). mTOR signaling in growth control and disease. *Cell* *149*, 274–293. <https://doi.org/10.1016/j.cell.2012.03.017>.

Lee, D.S., Gona, P., Vasani, R.S., Larson, M.G., Benjamin, E.J., Wang, T.J., Tu, J.V., and Levy, D. (2009). Relation of disease pathogenesis and risk factors to heart failure with preserved or reduced ejection fraction: insights from the Framingham heart study of the National Heart, Lung, and Blood Institute. *Circulation* *119*, 3070–3077. <https://doi.org/10.1161/CIRCULATIONAHA.108.815944>.

Li, J., Minami, I., Shiozaki, M., Yu, L., Yajima, S., Miyagawa, S., Shiba, Y., Morone, N., Fukushima, S., Yoshioka, M., et al. (2017). Human pluripotent stem cell-derived cardiac tissue-like constructs for repairing the infarcted myocardium. *Stem Cell Rep.* *9*, 1546–1559. <https://doi.org/10.1016/j.stemcr.2017.09.007>.

Lorenz, L., Axnick, J., Buschmann, T., Henning, C., Urner, S., Fang, S., Nurmi, H., Eichorst, N., Holtmeier, R., Bódis, K., et al. (2018). Mechanosensing by  $\beta 1$  integrin induces angiocrine signals for liver growth and survival. *Nature* *562*, 128–132. <https://doi.org/10.1038/s41586-018-0522-3>.

Lundy, S.D., Zhu, W.-Z., Regnier, M., and Laflamme, M.A. (2013). Structural and functional maturation of cardiomyocytes derived from human pluripotent stem cells. *Stem Cells Dev.* *22*, 1991–2002. <https://doi.org/10.1089/scd.2012.0490>.



- Matsuura, K., Wada, M., Shimizu, T., Haraguchi, Y., Sato, F., Sugiyama, K., Konishi, K., Shiba, Y., Ichikawa, H., Tachibana, A., et al. (2012). Creation of human cardiac cell sheets using pluripotent stem cells. *Biochem. Biophys. Res. Commun.* *425*, 321–327. <https://doi.org/10.1016/j.bbrc.2012.07.089>.
- Meiry, G., Reisner, Y., Feld, Y., Goldberg, S., Rosen, M., Ziv, N., and Binah, O. (2001). Evolution of action potential propagation and repolarization in cultured neonatal rat ventricular myocytes. *J. Cardiovasc. Electrophysiol.* *12*, 1269–1277. <https://doi.org/10.1046/j.1540-8167.2001.01269.x>.
- Nguyen, K., Yan, Y., Yuan, B., Dasgupta, A., Sun, J., Mu, H., Do, K.A., Ueno, N.T., Andreeff, M., and Battula, V.L. (2018). ST8SIA1 regulates tumor growth and metastasis in TNBC by activating the FAK-AKT-mTOR signaling pathway. *Mol. Cancer Ther.* *17*, 2689–2701. <https://doi.org/10.1158/1535-7163.MCT-18-0399>.
- Polyakova, V., Loeffler, I., Hein, S., Miyagawa, S., Piotrowska, I., Dammer, S., Risteli, J., Schaper, J., and Kostin, S. (2011). Fibrosis in endstage human heart failure: severe changes in collagen metabolism and MMP/TIMP profiles. *Int J Cardiol* *151*, 18–33. <https://doi.org/10.1016/j.ijcard.2010.04.053>.
- Ribeiro, M.C., Tertoolen, L.G., Guadix, J.A., Bellin, M., Kosmidis, G., D'Aniello, C., Monshouwer-Kloots, J., Goumans, M.J., Wang, Y.L., Feinberg, A.W., et al. (2015). Functional maturation of human pluripotent stem cell derived cardiomyocytes in vitro—Correlation between contraction force and electrophysiology. *Biomaterials* *51*, 138–150. <https://doi.org/10.1016/j.biomaterials.2015.01.067>.
- Sakai, S., Mishima, H., Ishii, T., Akaogi, H., Yoshioka, T., Ohyabu, Y., Chang, F., Ochiai, N., and Uemura, T. (2009). Rotating three-dimensional dynamic culture of adult human bone marrow-derived cells for tissue engineering of hyaline cartilage. *J. Orthop. Res.* *27*, 517–521. <https://doi.org/10.1002/jor.20566>.
- Sargent, C.Y., Berguig, G.Y., Kinney, M.A., Hiatt, L.A., Carpenedo, R.L., Berson, R.E., and McDevitt, T.C. (2010). Hydrodynamic modulation of embryonic stem cell differentiation by rotary orbital suspension culture. *Biotechnol. Bioeng.* *105*, 611–626. <https://doi.org/10.1002/bit.22578>.
- Schwarz, R.P., Goodwin, T.J., and Wolf, D.A. (1992). Cell culture for three-dimensional modeling in rotating-wall vessels: an application of simulated microgravity. *J. Tissue Cult. Methods* *14*, 51–57. <https://doi.org/10.1007/BF01404744>.
- Sciarretta, S., Volpe, M., and Sadoshima, J. (2014). Mammalian target of rapamycin signaling in cardiac physiology and disease. *Circ. Res.* *114*, 549–564. <https://doi.org/10.1161/CIRCRESAHA.114.302022>.
- Sekiya, N., Matsumiya, G., Miyagawa, S., Saito, A., Shimizu, T., Okano, T., Kawaguchi, N., Matsuura, N., and Sawa, Y. (2009). Layered implantation of myoblast sheets attenuates adverse cardiac remodeling of the infarcted heart. *J. Thorac. Cardiovasc. Surg.* *138*, 985–993. <https://doi.org/10.1016/j.jtcvs.2009.02.004>.
- Shimizu, T., Sekine, H., Yang, J., Isoi, Y., Yamato, M., Kikuchi, A., Kobayashi, E., and Okano, T. (2006). Polysurgery of cell sheet grafts overcomes diffusion limits to produce thick, vascularized myocardial tissues. *FASEB J.* *20*, 708–710. <https://doi.org/10.1096/fj.05-4715fje>.
- Teo, A., Mantalaris, A., Song, K., and Lim, M. (2014). A novel perfused rotary bioreactor for cardiomyogenesis of embryonic stem cells. *Biotechnol. Lett.* *36*, 947–960. <https://doi.org/10.1007/s10529-014-1456-y>.
- Tohyama, S., Hattori, F., Sano, M., Hishiki, T., Nagahata, Y., Matsuura, T., Hashimoto, H., Suzuki, T., Yamashita, H., Satoh, Y., et al. (2013). Distinct metabolic flow enables large-scale purification of mouse and human pluripotent stem cell-derived cardiomyocytes. *Cell Stem Cell* *12*, 127–137. <https://doi.org/10.1016/j.stem.2012.09.013>.
- Urbich, C., Walter, D.H., Zeiher, A.M., and Dimmeler, S. (2000). Laminar shear stress upregulates integrin expression: role in endothelial cell adhesion and apoptosis. *Circ. Res.* *87*, 683–689. <https://doi.org/10.1161/01.res.87.8.683>.
- Weinberger, F., Breckwoldt, K., Pecha, S., Kelly, A., Geertz, B., Starbatty, J., Yorgan, T., Cheng, K.H., Lessmann, K., Stolen, T., et al. (2016). Cardiac repair in Guinea pigs with human engineered heart tissue from induced pluripotent stem cells. *Sci. Transl. Med.* *8*, 363ra148. <https://doi.org/10.1126/scitranslmed.aaf8781>.
- Wendel, J.S., Ye, L., Tao, R., Zhang, J., Kamp, T.J., and Tranquillo, R.T. (2015). Functional effects of a tissue-engineered cardiac patch from human induced pluripotent stem cell-derived cardiomyocytes in a rat infarct model. *Stem Cells Transl. Med.* *4*, 1324–1332. <https://doi.org/10.5966/sctm.2015-0044>.
- Xia, H., Nho, R.S., Kahm, J., Kleidon, J., and Henke, C.A. (2004). Focal adhesion kinase is upstream of phosphatidylinositol 3-kinase/AKT in regulating fibroblast survival in response to contraction of type I collagen matrices via a beta 1 integrin viability signaling pathway. *J. Biol. Chem.* *279*, 33024–33034. <https://doi.org/10.1074/jbc.M313265200>.
- Yang, X., Pabon, L., and Murry, C.E. (2014). Engineering adolescence: maturation of human pluripotent stem cell-derived cardiomyocytes. *Circ. Res.* *114*, 511–523. <https://doi.org/10.1161/CIRCRESAHA.114.300558>.
- Yoshida, S., Miyagawa, S., Fukushima, S., Kawamura, T., Kashiyama, N., Ohashi, E., Toyofuku, T., Toda, K., and Sawa, Y. (2018). Maturation of human induced pluripotent stem cell-derived cardiomyocytes by soluble factors from human mesenchymal stem cells. *Mol. Ther.* *26*, 2681–2695. <https://doi.org/10.1016/j.ymthe.2018.08.012>.
- You, D., Xin, J., Volk, A., Wei, W., Schmidt, R., Scurti, G., Nand, S., Breuer, E.K., Kuo, P.C., Breslin, P., et al. (2015). FAK mediates a compensatory survival signal parallel to PI3K-AKT in PTEN-null T-ALL cells. *Cell Rep.* *10*, 2055–2068. <https://doi.org/10.1016/j.cellrep.2015.02.056>.
- Zhang, J., Wilson, G.F., Soerens, A.G., Koonce, C.H., Yu, J., Palecek, S.P., Thomson, J.A., and Kamp, T.J. (2009). Functional cardiomyocytes derived from human induced pluripotent stem cells. *Circ. Res.* *104*, e30–41. <https://doi.org/10.1161/CIRCRESAHA.108.192237>.